Submitted to ADVANCED MATERIALS

Supporting Information

Synthesis of Size-tunable Polymeric Nanoparticles Enabled by 3D Hydrodynamic Flow Focusing in Single-Layer Microchannels

By *Minsoung Rhee*[1,2,3,†], *Pedro M. Valencia*[4,†], *Maria I. Rodriguez*[5], *Robert Langer*[3,4,6], *Omid C. Farokhzad*[2,6,*], *Rohit Karnik*[1,*]

[1]Department of Mechanical Engineering, Massachusetts Institute of Technology, Cambridge, MA 02139. [2]Laboratory of Nanomedicine and Biomaterials and Department of Anesthesiology, Brigham and Women's Hospital, Harvard Medical School, Boston, MA 02115. [3]David H. Koch Institute for Integrative Cancer Research, Massachusetts Institute of Technology, Cambridge, MA 02139. [4]Department of Chemical Engineering, Massachusetts Institute of Technology, Cambridge, MA 02139. [5]Department of Electrical Engineering and Computer Science, Massachusetts Institute of Technology, Cambridge, MA 02139. [6]MIT-Harvard Center for Cancer Nanotechnology Excellence, Massachusetts Institute of Technology, Cambridge, MA 02139.

Contents

1. Mathematical Analysis for flat-profile flow

Here, we describe a mathematical model of the vertical focusing section of the 3D HFF device. Since flow in the channel prior to horizontal focusing by the water streams is more than an order of magnitude slower than that following focusing by the water sheath streams, diffusion in the channel prior to focusing determines the polymer wall concentrations when the organic stream is focused by the water sheath streams. Furthermore, in our design, the channel width decreases from 100 μm to 20 μm just prior to focusing by the water sheath streams. Since the flow velocity is much higher in the 20 μm channel just prior to focusing, we do not consider diffusion in this section (see focusing length *L* in Figure 1).
The governing transport equation for the vertical single-phase hydrodynamic focusing system is given by

$$\frac{\partial c}{\partial t}+\left(u\frac{\partial c}{\partial x}+v\frac{\partial c}{\partial y}+w\frac{\partial c}{\partial z}\right)=D\left(\frac{\partial^2 c}{\partial x^2}+\frac{\partial^2 c}{\partial y^2}+\frac{\partial^2 c}{\partial z^2}\right), \tag{1}$$

where c is the sample concentration, *u*, *v*, and *w* are velocity components in x, y and z directions, and D is the diffusion coefficient of the sample in the solvent. The time dependency in Eq. (1) is neglected since the hydrodynamic focusing occurs in continuous systems. Diffusion in the *x*-direction is negligible compared to high convection in the same direction. We also assumed constant concentrations in the *y*-direction as in the case of two infinite parallel plates since channel aspect ratio ($w/h >> 1$) , which subsequently removes the *y*-dependency in Eq. (1). The simplified governing equation is then given by

$$u\frac{\partial c}{\partial x}=D\frac{\partial^2 c}{\partial z^2} \tag{2}$$

A further simplification by assuming a flat uniform velocity, u_{max}, across the channel is valid when the channel aspect ratio (w/h) is high enough (>>1) and gives the mass transport equation as

$$u_{\max}\frac{\partial c}{\partial x}=D\frac{\partial^2 c}{\partial z^2} \tag{3}$$

with initial and boundary conditions as follows.

$$c = c_{\max} \qquad 0 \le z \le h_f \tag{4}$$

$$c = 0 \qquad h_f < z \le h\,. \tag{5}$$

$$\frac{\partial c}{\partial x} = 0 \qquad at\ z = h\,. \tag{6}$$

$$\frac{\partial c}{\partial x} = 0 \qquad at\ z = 0\,. \tag{7}$$

Substituting Eq. (3) with its dimensionless forms gives a non-dimensionalized governing equation as

$$\frac{\partial \theta}{\partial X} = \frac{\partial^2 \theta}{\partial Z^2} \tag{8}$$

where

$$\theta = c / c_{\max},\ X = x / Pe \cdot h, Pe = u_{\max} \cdot h / D\ and\ Z = z / h\,. \tag{9}$$

By separation of variables, the solution to Eq. (8) is found to be

$$\theta(x,z) = \frac{c}{c_{\max}} = \frac{h_f}{h} + \sum_{n=1}^{\infty} \frac{2}{n\pi} \sin\left(n\pi \frac{h_f}{h}\right) \exp\left(-n^2\pi^2 \frac{x}{Pe \cdot h}\right) \cos\left(n\pi \frac{z}{h}\right) \tag{10}$$

Figure S-1 shows the variation of dimensionless wall concentrations along the vertical focusing channel at various sample flow rate fractions (*f*), when the flow velocity is assumedly flat. When the velocity of a flow becomes flat across the channel, the focused stream will be less squeezed,

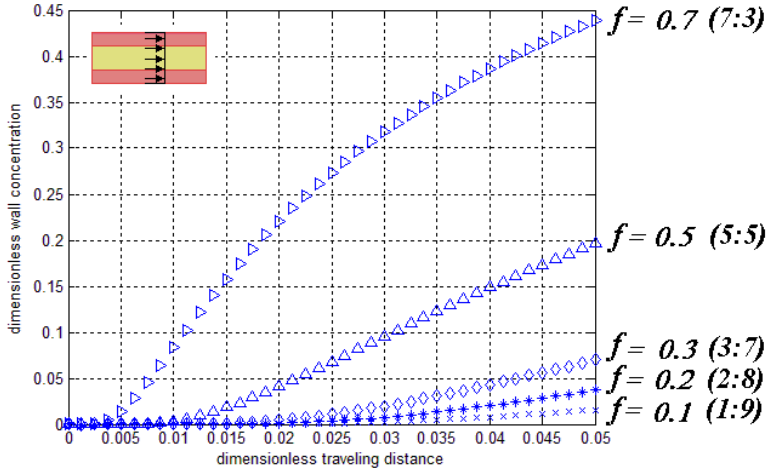

Figure S-1. Mathematical predictions on the variations of the dimensionless wall concentration along the vertical focusing channel at various sample/sheath flow rate ratios (*f*) with the solute concentration and the total flow rate fixed, when the velocity profile is assumed flat with a constant velocity.

resulting in a thicker focused stream than the real focused stream, but the effect of axial convection near the wall will be increased, making solutes near the wall move faster along the channel. These two different effects will compensate for each other, and thus assumption of a flat velocity profile gives much simpler and quicker mathematical analysis with sufficiently accurate estimations than the more accurate solution for the parabolic velocity profile model.

2. Modified *Péclet* number as an indicator of aggregation

The modified *Péclet* number is defined as a product of the *Péclet* number and the ratio of channel height to focusing length (h/L), which takes into account the relative importance of convection to diffusion of the polymer precursor. The focusing length (L) in Figure 1 starts from the position where focused stream enters and ends where the channel becomes narrow. This is because the narrowed channel makes *Pe* significantly higher, which, in turn, imples that there will be almost no change in polymer concentration in the narrowed channel. When the hydrodynamic flow focusing occurs in microchannels, it will change the diffusion timescale due to the squeezed center stream. The focusing *Péclet* number (Pe_f), a ratio of

diffusive timescale for the sheath layer to convective timescale along the channel length, can be then defined as

$$Pe_f = \frac{t_{diff}}{t_{conv}} = \frac{(h-h_f)^2/2D}{L/u_{ave}} = \frac{h^2(1-f)^2/2D}{3L/2u_{\max}} = \frac{1}{3}\left(\frac{u_{\max}\cdot h}{D}\right)\left(\frac{h}{L}\right)(1-f)^2. \quad (11)$$

The focusing *Péclet* number may determine how efficiently the polymer precursors will be retained out of the channel wall during the course of travel. As Pe_f increases, the distance diffused by the polymer decreases for a given precipitation time, thereby diminishing the chance of aggregation. When Pe_f approaches to 1, the diffusive timescale becomes comparable to the convective timescale, which implies a significant increase in wall concentrations for the same time course, resulting in more susceptibility to aggregation. Similarly, a larger channel height or smaller polymer flow ratio increases the distance between the polymer stream and the channel top and bottom, again decreasing the susceptibility to aggregation. However, higher flow rates will generate larger pressure drops along the channel and thus increase the chance of device failure. In addition, microfabrication of the device always imposes a technical limitation on the channel aspect ratio (width to height) that constrains the channel height for a given width.

3. Simulations with 2D geometry

To reduce the computational demand, most of the simulations can be done in 2D geometry without significant loss of accuracy compared to 3D simulations that requires substantially more resources. In **Figure S-2**, the vertical focusing progress in a straight channel for various flow rate ratios was simulated. The vertically focused stream remains for an extended time around the centerline and gradually diffuses into both sheath streams, eventually reaching at

the top and bottom walls. Note that the sample stream will be lifted upward by the bottom sheath stream first and then will be pushed downward by the top sheath stream. This difference in the contact order makes the sample diffuse out to the bottom slightly faster than to the top (**Figure S-3a**). **Figure S-3b** shows a good agreement between the simulated wall concentration change along the channel and the corresponding results calculated by mathematical modeling.

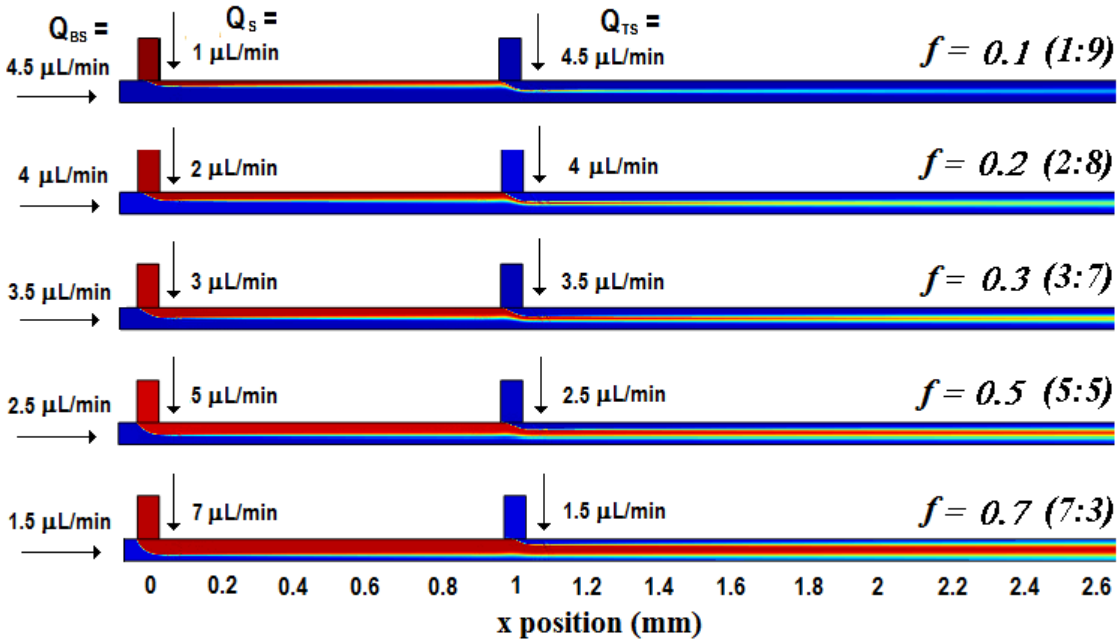

Figure S-2. Two-dimensional simulations showing the vertical focusing progress in a straight channel for various flow rate fractions (*f*).

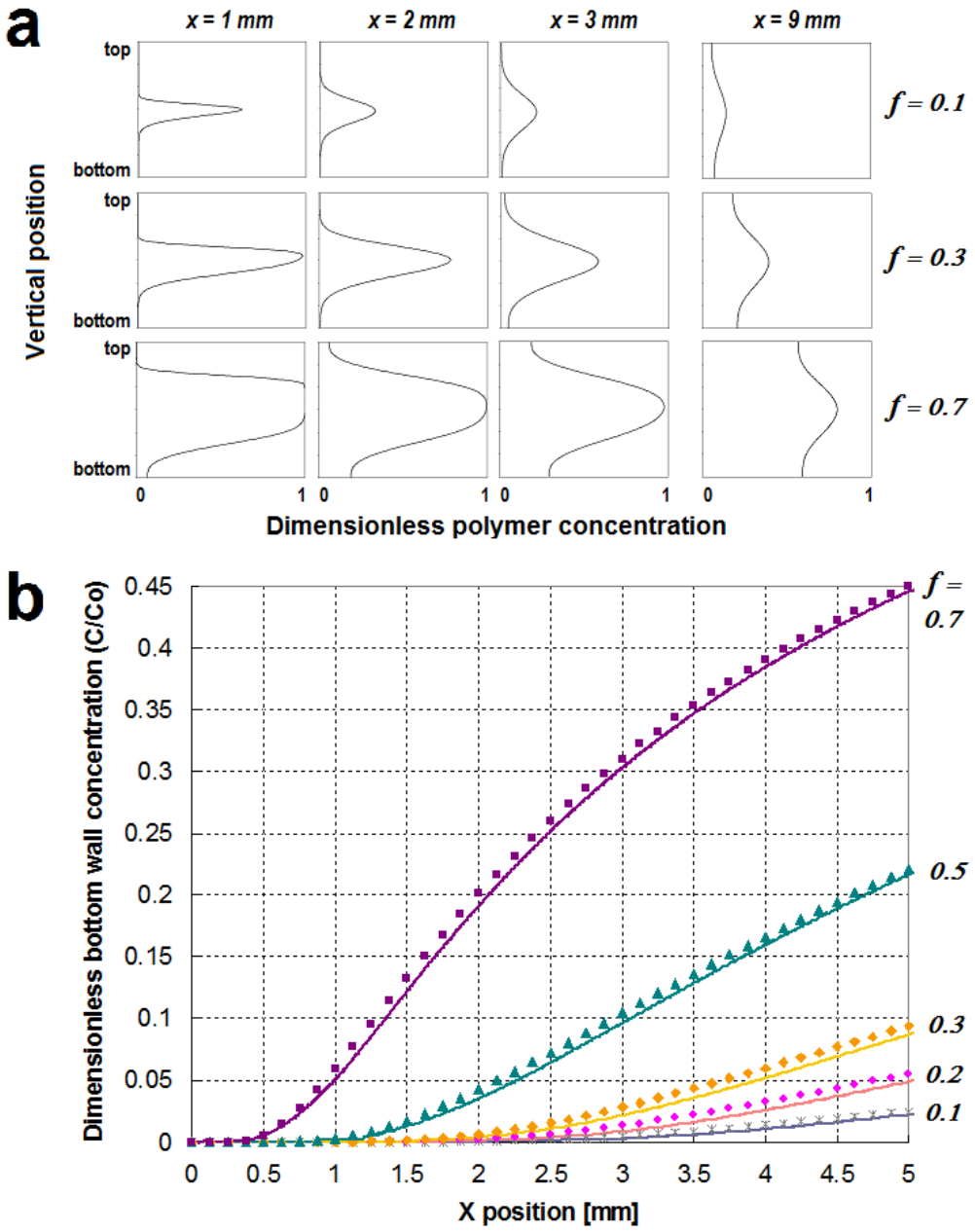

Figure S-3. 2D simulations showing the development and fade-out of vertical focusing in a straight channel for various flow rate ratios. (a) Polymer solute distributions depending on the flow rate ratio and the distance that the combined flow travels in the x-direction. (b) Bottom wall concentration changes along the channel depending on the flow rate ratio. Solid lines represent simulated results from 2D simulations while markers are shown based on mathematical predictions.

For higher sample flow rate fractions (*f*), the wall concentration increases more rapidly. Therefore, sample solutes can be vertically isolated for longer time when its flow rate ratio to sheath flows is low. However, for low sample flow rate ratios, the solute concentration of the

focused stream decreases faster as can be seen in **Figure S-4**. In other words, the focused stream with a low flow rate ratio tends to lose its precursor molecules more quickly by diffusion and become diluted rapidly.

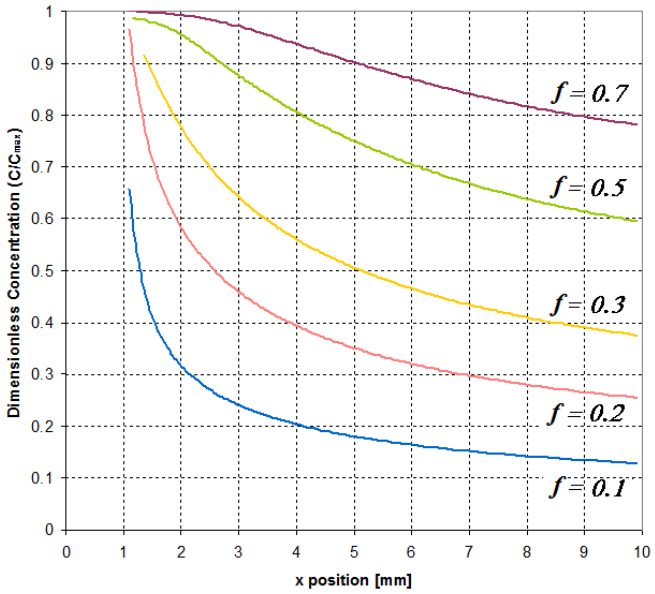

Figure S-4. Two-dimensional simulations showing the change in the centerline concentration depending on the flow rate ratio during the vertical focusing progress in a straight channel.

4. SEM images of the device

The size and position of inlet holes play a critical role in determining the shape of hydrodynamic focusing in the channel. **Figure S-5** shows typical inlet holes constructed within vertical focusing channels by a mechanical drill capable of positioning x and y locations precisely.

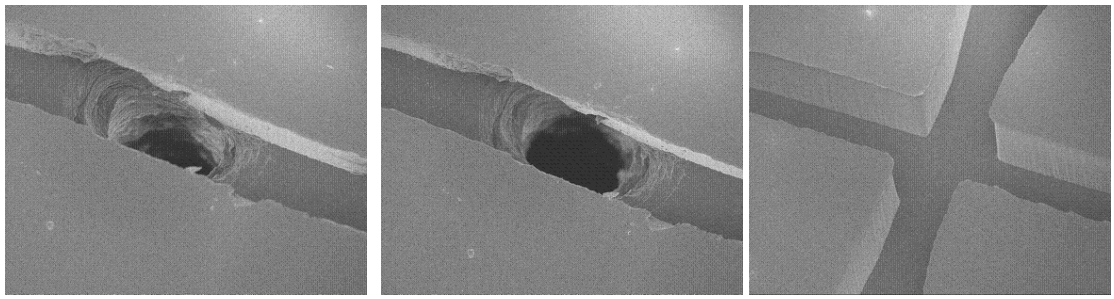

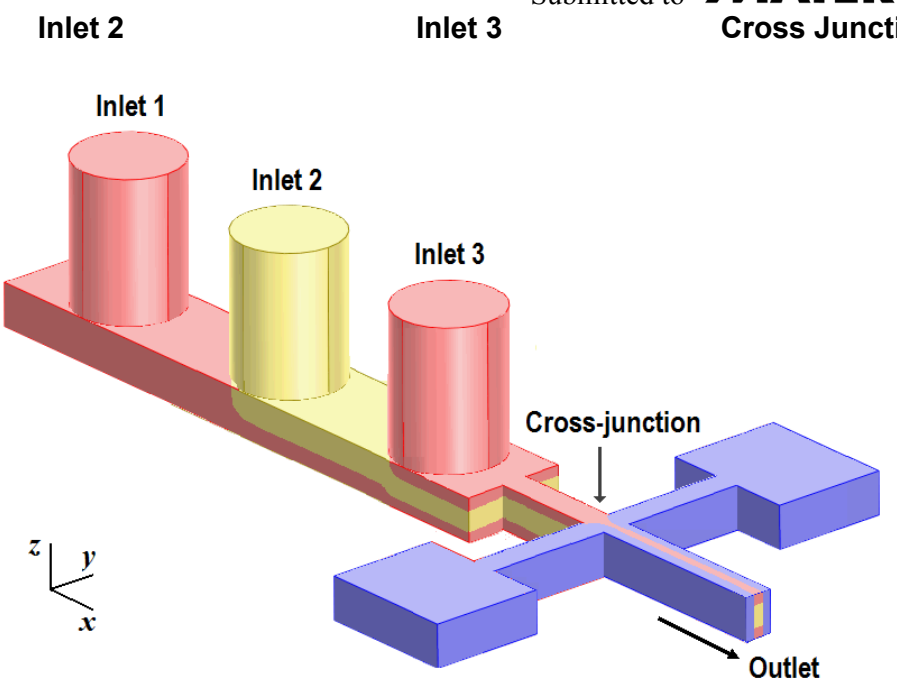

Figure S-5. SEM images of inlet holes and a cross junction of the sequential hole 3D HFF device.

5. Visualizations of aggregation occurring during 2D HFF

In **Figure S-6**, the PLGA precursor solution with molecular weight of ~ 70,000 was prepared in acetonitrile at a concentration of 10 mg mL^{-1}. Wall adsorption and aggregation began only a few seconds after the stream was introduced. By the time of a few minutes, the PLGA precipitate becomes large enough to block the channel. However, 3D hydrodynamic focusing with three sequential holes provided a robust and consistent means to successfully synthesize PLGA nanoparticles from the equivalent condition without any complications such as channel block or wall adsorption. Movie clips showing how aggregation blocks the channel during 2D HFF are also available online from Wiley InterScience or from the author.

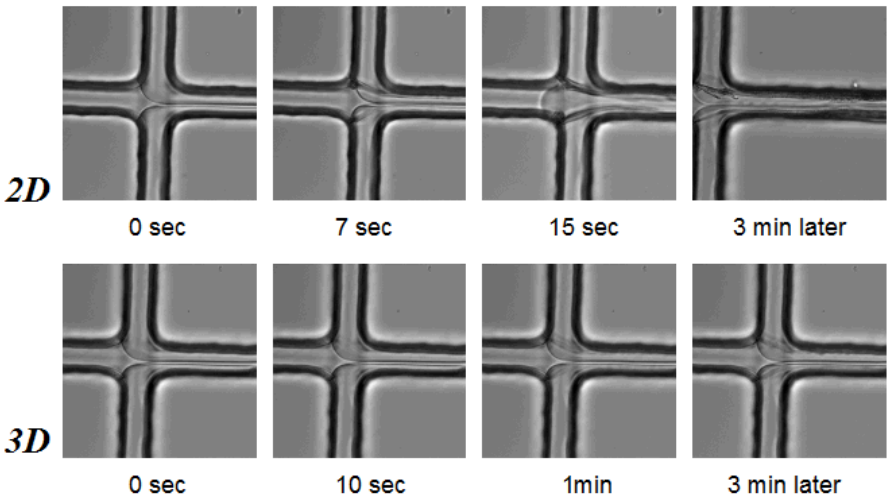

Figure S-6. Growth of PLGA particles and its effects on the channel. During 2D hydrodynamic focusing, vigorous aggregation of PLGA particles occurs within a minute. Agglomerated PLGA microparticles stick to the walls and block the entire channel after a few minutes (Top panel). During 3D hydrodynamic focusing with the equivalent conditions, successful synthesis of PLGA nanoparticles was observed without channel block or wall adsorption (Bottom panel).

6. Synthesis of PLGA and PLGA-PEG NPs

Figure S-7 shows how PLGA particles easily grow and aggregate on the channel wall when they encounter the anti-solvent (water) under the Phase II conditions (similar aggregation also occurs in 2D HFF). 3D HFF under Phase I conditions, however, provided a robust and predictable means to successfully synthesize PLGA nanoparticles at the equivalent condition without any aggregation.

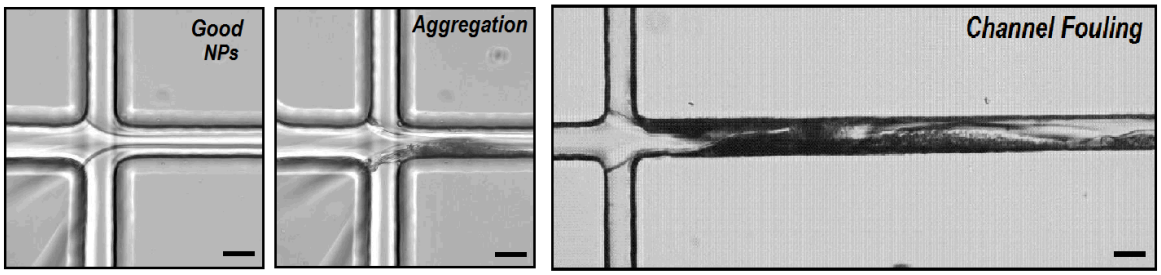

Figure S-7. Synthesis of PLGA NPs from pure $PLGA_{70K}$ precursors (10 mg mL^{-1}) by 3D HFF for varying operation parameters. (a) Channel image at the conditions that result good synthesis of NPs and (b) that are susceptible to aggregation. (c) Channel fouling due to long-term aggregation of PLGA microparticles (bottom) (scale bars 20 μm).

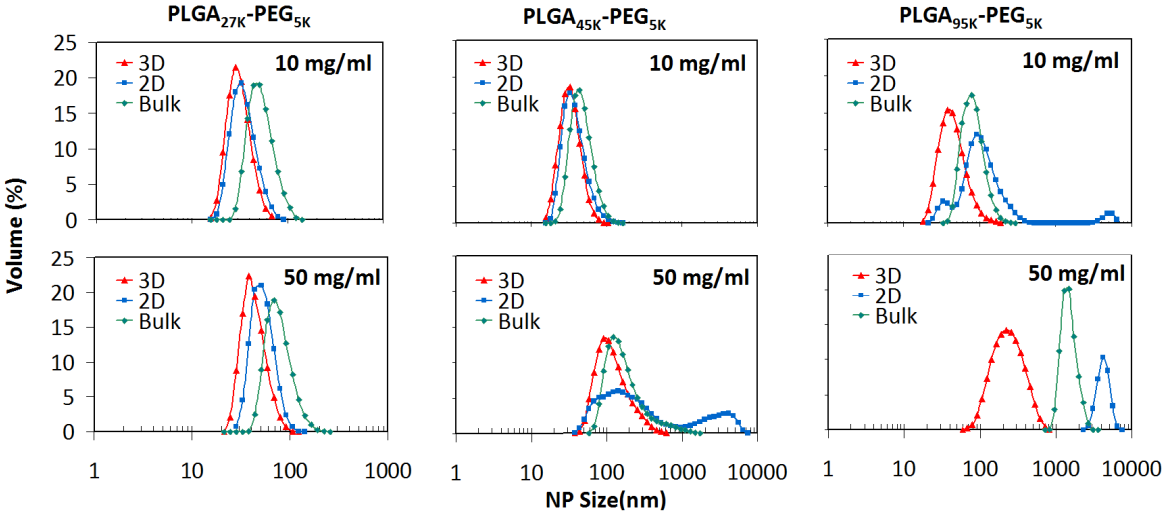

Figure S-8. Comparison of size distributions by volume fraction of PLGA-PEG NPs prepared by microfluidic 3D HFF, 2D, and bulk mixing methods for the precursor concentrations of 10 (low) and 50 mg mL^{-1} (high), respectively. Aggregated particles are found in the 1000-10,000 nm range.

Figure S-8 shows the size distributions of NPs made from various MW polymer precursors at low and high concentrations (10mg/mL and 50mg/mL, respectively) using the three different methods. At high concentrations, NPs obtained by 2D HFF and bulk methods yielded highly polydisperse particles of extremely large size (>1000 nm), while the implementation of 3D HFF consistently resulted in smaller NPs with relatively low polydispersity regardless of polymer concentrations. These observations indicate that 2D HFF is comparable with 3D HFF only for small MW polymers or very low polymer concentrations where the channels are less susceptible to fouling.

Aggregated particles are larger and thus reflect more light so that the solution with aggregated particles can look opaque. **Figure S-9** shows direct visualization of collected sample solutions that contain synthesized PLGA-PEG particles with various sizes.

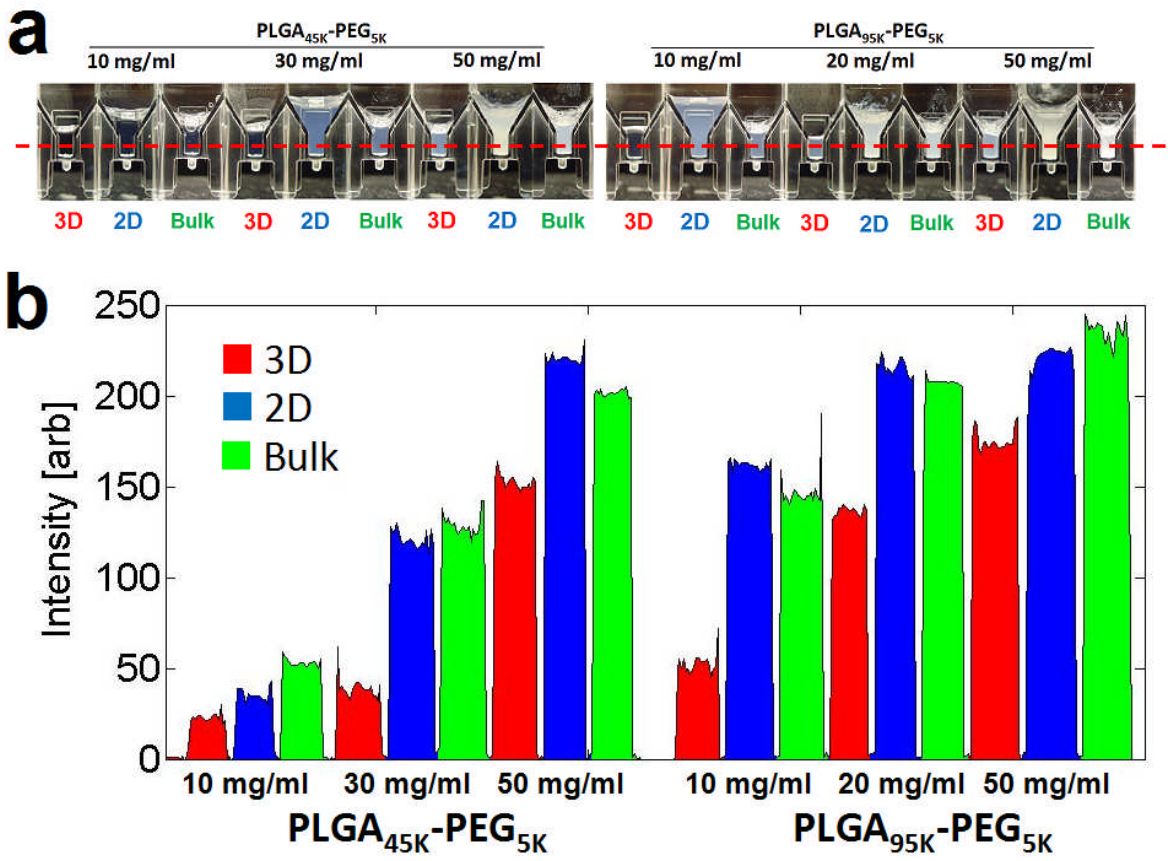

Figure S-9. Synthesis of various PLGA-PEG NPs. (a) Photos of NP solutions prapared by 3D HFF, 2D HFF, and bulk synthesis. Opacity of the solution roughly indicates the average size of NPs in the solution. Clear solutions contain small NPs (< ~50 nm) and opaque solutions have large particles up to several microns. (b) Calculated light intensity along the red dashed line in (a) to estimate the opacity of the solutions.

7. Experimental

Polymer Precursors. For PLGA NPs , a solution of PLGA (inherent viscosity 0.82 dL g^{-1}, molecular weight ~ 70,000; Lactel, Pelham, AL) was dissolved in ACN at varying concentrations from 0.5 to 10 mg mL^{-1}). For PLGA-PEG NPs, solutions of PLGA-PEG (Boehringer Ingelheim GmbH, Germany) at molecular weights of $PLGA_{27K}$-PEG_{5K}, $PLGA_{45K}$-PEG_{5K}, and $PLGA_{95K}$-PEG_{5K} were dissolved in ACN at concentrations of 10-50 mg mL^{-1}.

Device Fabrication. The prototypical device was manufactured using the standard soft-lithographic technique. The SU-8 (MicroChem) resist was spun on a bare 4" silicon wafer and prebaked on a hot plate for 3 min at 65 °C and for 9 min subsequently at 95 °C. After exposure to 365 nm UV light, the coated wafer was postbaked for 1 min at 65 °C and for 7 min subsequently at 95 °C. The successive 4 min development resulted in the 60 μm thick mold. PDMS (Sylgard 184, Dow Corning) monomer and curing agent were mixed in a ratio of 10:1 by weight, poured over the silicon wafer mold, and degassed. After curing at 100 °C for 60 min, the cured PDMS cast was carefully removed from the mold and diced into individual dies. For each die, inlet/outlet holes were drilled by a 150 μm diameter drill bit. To prevent holes drilled at off-center positions, a manual travel translation stage was used with a mechanical drill to define the position precisely. The PDMS component was then bonded to a 1 in. × 2 in. glass slide using air plasma. Typical channel dimensions used in the NP synthesis experiments had a width of 100 μm and a height of 60 μm for the vertical focusing part and had a width of 20 μm for the horizontal focusing part, or precipitation channel.

Fluid Control and NP synthesis. For 3D HFF, A 2.500 mL syringe for water injection was mounted on a syringe pump (SP101I, World Precision Instruments), two 500 μL syringes for ACN injection were mounted on a different syringe pump (PHD 2000, Harvard Apparatus), and finally a 250 μL syringe for polymer solution injection was mounted on a syringe pump (PHD ULTRA, Harvard Apparatus). Water and organic flow rates were maintained at 50 μL min^{-1} and 10 μL min^{-1}, respectively (60 μL min^{-1} in total), while the fraction of polymer flow rates in the organic flow were varied from 0.1 to 1. To prepare NPs by 2D HFF we used a channel design previously published [5] and ran a polymer stream at different concentrations at an organic to aqueous flow ratio of 1:10. For 3D and 2D, we used devices with the exactly same dimensions, and all flow rates were also identical. The water flow rate was always 50

μL min^{-1} for both 3D and 2D, and the organic flow rate was always 10 μL min^{-1} for both 3D and 2D. For example, for 3D HFF with polymeric stream 3 μL min^{-1} and total ACN sheath 7 μL min^{-1} (f = 0.3) for a net organic flow rate of10 μL min^{-1}, the corresponding 2D HFF polymeric stream flow rate was 10 μL min^{-1}. Consequently, the width of the organic stream focused by the water sheath streams, fluid velocities, and residence times were the same for 3D and 2D. The average fluid velocity for the vertical focusing region was approximately 0.028 m s^{-1}. The corresponding residence time for this 1.5 mm vertical focusing region was about 54 ms. The average fluid velocity in the following precipitation channel was 0.83 m s^{-1} and the residence time for 4 mm long precipitation channel was about 4.8 ms. The total residence time for polymeric molecules in the microfluidic channel was ~58.8 ms. Reynolds numbers for precipitation and vertical focusing channels were 16.6 and 3.5, respectively. In bulk, we mixed 200 μL of polymer precursor solution drop-wise with 2mL of water during 1-2 hrs. NPs were measured immediately after. It was also noticed that NPs size did not varied significantly after washing NPs with water several times.

Particle Sizing. Particle sizing was performed using dynamic light scattering with Zetasizer Nano ZS (Malvern Instruments Ltd., U.K.). For each measurement, 100 μL or more volume of the sample was loaded in a disposable low-volume cuvette. More than three measurements were performed on each sample. All measurements were performed at ACN concentrations of less than 10% ACN to ensure that any observed variation in particle size was not due to the solvent.

Transmission Electron Microscopy (TEM). TEM experiments were carried out on a JEOL JEM-2011 instrument at an acceleration voltage of 200 kV. The TEM sample was prepared by depositing 10 μL of the NP suspension (1.0 mg mL^{-1}) onto a 300-mesh carbon-coated copper grid. Samples were blotted away after 30 min incubation and grids were negatively stained for 20 min at the room temperature with sterile-filtered 3% (w/v) uranyl acetate aqueous solution. The grids were then washed twice with distilled water and air dried prior to imaging.

Image Acquisition. For confocal imaging, a Zeiss LSM 510 Laser Scanning Confocal microscope (Carl Zeiss MicroImaging, Inc., Thornwood, NY) was used. Microfluidic device was mounted on a thin cover slip and with corresponding tubing for inlets and outlets. A FITC solution was used for the focused stream at flow rates of 1-5 μL min^{-1} and a rhodamine solution was used for the vertical sheath streams at flow rates of 5-9 μL min^{-1}. Water stream was not labeled. For each combination of flow rates a z-stack of 165 images was taken at 0.76 μm per z-sectioning step at different regions of the channel. Lasers at 488 nm and 543 nm wavelengths were used together with 25x objective. For nanoparticle synthesis the experiments were performed on the device oriented on a stage of a stereomicroscope (Nikon Eclipse TE 2000U).

Simulation Methods. Two-dimensional and three-dimensional simulations were performed using COMSOL Multiphysics software, a commercial finite element package (COMSOL Inc., Burlington, MA). The flow rates at the bottom, polymer, and top inlets were 3.5, 3, and 3.5 μL/min, respectively, as were used in the experiments. After flow profiles in the channel were obtained by solving the incompressible Navier-Stokes equation, concentration profiles were separately calculated by solving the Convection and Diffusion equation. The diffusion coefficient of the polymeric solute ($PLGA_{70K}$) in ACN used in the simulations ($D \sim 1.95 \times 10^{-10}$ m^2 s^{-1}) was based on the value estimated from the Einstein-Stokes equation (ACN viscosity ~ 0.38 cp, radius of gyration of PLGA precursors ~ 4-5 nm) and further comparison with the data for similar molecules.